







Understanding FRB 200428 in the Synchrotron Maser Shock Model: Consistency and Possible Challenge

Q. Wu¹ , G. Q. Zhang¹ , F. Y. Wang^{1,2} , and Z. G. Dai^{1,2} 

¹School of Astronomy and Space Science, Nanjing University, Nanjing 210093, People's Republic of China; fayinwang@nju.edu.cn

²Key Laboratory of Modern Astronomy and Astrophysics (Nanjing University), Ministry of Education, Nanjing 210093, People's Republic of China
Received 2020 June 29; revised 2020 August 11; accepted 2020 August 12; published 2020 September 4

Abstract

Recently, the discovery of Galactic FRB 200428 associated with an X-ray burst (XRB) of SGR 1935+2154 has built a bridge between FRBs and magnetar activities. In this Letter, we assume that the XRB occurs in the magnetar magnetosphere. We show that the observational properties of FRB 200428 and the associated XRB are consistent with the predictions of synchrotron maser emission at ultrarelativistic magnetized shocks, including radiation efficiency, similar energy occurrence frequency distributions, and simultaneous arrive times. It requires that the upstream medium is a mildly relativistic baryonic shell ejected by a previous flare. The energy injection by flares responsible for the radio bursts will produce a magnetar wind nebula, which has been used to explain the persistent radio source associated with FRB 121102. We find that the radio continuum around SGR 1935+2154 can be well understood in the magnetar wind nebula model, by assuming the same energy injection rate $\dot{E} \propto t^{-1.37}$ as FRB 121102. The required baryonic mass is also estimated from the observations of FRB 121102 by the Green Bank Telescope and the Five-hundred-meter Aperture Spherical Telescope. By assuming the same radiation efficiency $\eta \sim 10^{-5}$, the total baryonic mass ejected from the central magnetar is about 0.005 solar mass. This value is much larger than the typical mass of a magnetar outer crust, but is comparable to the total mass of a magnetar crust.

Unified Astronomy Thesaurus concepts: [Radio transient sources \(2008\)](#); [Radio bursts \(1339\)](#); [Magnetars \(992\)](#); [Soft gamma-ray repeaters \(1471\)](#)

1. Introduction

Fast radio bursts (FRBs) are short and intense bursts of radio waves that suddenly appear in the distant universe, with a few milliseconds duration (Lorimer et al. 2007; Thornton et al. 2013). Most of them are extragalactic events because their large dispersion measures (DMs) far exceed the contribution of the Milky Way (Cordes & Chatterjee 2019; Petroff et al. 2019). Although nine FRBs have been localized, the origin of FRBs are still unknown. Many theoretical models of FRBs have been proposed (Platts et al. 2019). The millisecond durations and huge energy releases of FRBs are suggestive of their central engines being stellar-mass compact objects such as magnetars (Popov & Postnov 2013; Kulkarni et al. 2014; Katz 2016; Murase et al. 2016; Beloborodov 2017; Metzger et al. 2017; Wang & Yu 2017; Lu & Kumar 2018; Yang & Zhang 2018; Wadiasingh & Timokhin 2019; Wang et al. 2020). The high linear polarization and large rotation measures of FRB 121102 also require a strongly magnetized central engine and environment (Michilli et al. 2018). Meanwhile, the statistical similarity, such as energy, duration, and waiting time, between FRB 121102 and Galactic magnetar flares supports the magnetar central engine (Wang & Yu 2017; Wadiasingh & Timokhin 2019; Cheng et al. 2020).

On 2020 April 28, FRB 200428 was observed to be emitted from the Galactic magnetar SGR 1935+2154 (Bochenek et al. 2020; The CHIME/FRB Collaboration et al. 2020). The double-peaked burst was temporally coincident with a double-peaked XRB with the same time separation (Li et al. 2020; Ridnaia et al. 2020). This association confirms the connection between FRBs and flare activities of magnetars. Interestingly, it is well known that solar type III radio bursts are usually associated with solar XRBs (Bastian et al. 1998; Reid & Ratcliffe 2014). The peak time of XRBs precedes the peaks of

solar radio burst by a few seconds (Bastian et al. 1998). Similar behaviors between FRBs and solar type III radio bursts have been found (Zhang et al. 2019). There are some theoretical works on this FRB (Dai 2020; Geng et al. 2020; Katz 2020; Lu et al. 2020; Lyutikov & Popov 2020; Margalit et al. 2020a; Yu et al. 2020; Yang et al. 2020). In this Letter, we focus on the synchrotron maser shock model proposed by Metzger et al. (2019). It has been shown that this model can explain the properties of cosmological FRBs (Metzger et al. 2019; Margalit et al. 2020b). Whether FRB 200428 can be explained by this model is still under debate (Lu et al. 2020; Margalit et al. 2020a; Yu et al. 2020; Wang 2020).

In this Letter, we use the latest observations to test the parameters of the synchrotron maser shock model and discuss its consistency and the challenges. This Letter is organized as follows. In Section 2, we introduce the observations of FRB 200428 and SGR 1935+2154. In Section 3, the parameter constraints on the synchrotron maser model are given. The energy frequency distributions of FRBs and XRBs of SGR 1935+2154 are discussed in Section 4. In Section 5, we discuss the rotation measure and the persistent radio source of FRB 121102 and FRB 200428. In Section 6, the baryon mass required by the synchrotron maser model is estimated. A summary is given in Section 7.

2. Observational Properties of SGR 1935+2154 and FRB 200428

2.1. SGR 1935+2154

SGR 1935+2154 is a Galactic magnetar, which sprayed a short burst first detected by Swift/Burst Alert Telescope (BAT), on 2014 July 5 (Stamatikos et al. 2014; Lien et al. 2014). After that, different telescopes, including Swift/X-ray Telescope, Chandra, and XMM-Newton X-ray observations,

carried out continuous observation of X-ray pulsations, and confirmed that the source is a typical magnetar with a spin period $P \sim 3.24$ s, a spin-down rate $\dot{P} \simeq 1.43 \times 10^{-11}$ s s $^{-1}$, and a surface dipolar magnetic field strength of $B \sim 2.2 \times 10^{14}$ G (Israel et al. 2016). This source may be associated with the supernova remnant (SNR) G57.2+0.8. The distance of SGR 1935+2154 has a large range, i.e., from 4.5 to 12.5 kpc (Israel et al. 2016; Kothes et al. 2018; Zhou et al. 2020; Zhong et al. 2020). In this Letter, we adopt the distance of $d = 9$ kpc.

Since 2020 April, multiple short and bright bursts have made up a burst forest, which means SGR 1935+2154 has entered a new active period (Hurley et al. 2020; Veres et al. 2020). Luminous hard X-ray bursts were observed by INTEGRAL (Mereghetti et al. 2020), AGILE (Tavani et al. 2020), Konus-Wind (Ridnaia et al. 2020), and Insight-HXMT (Li et al. 2020), respectively. The light curve of the XRB shows two narrow peaks with an interval of about 30 ms (Ridnaia et al. 2020; Li et al. 2020), which is consistent with the separation time between the two narrow peaks in FRB 200428. The total fluence of the XRB, measured by Konus-Wind in the 20,500 keV band, is $F_X = (9.7 \pm 1.1) \times 10^{-7}$ erg cm $^{-2}$. The peak energy flux is $S_X = (7.5 \pm 1.0) \times 10^{-6}$ erg cm $^{-2}$ s $^{-1}$, in a 16 ms time interval (Ridnaia et al. 2020). For the distance of $d = 9$ kpc, the burst energy in X-rays is

$$E_X = 4\pi F_X d^2 = 9.4 \times 10^{39} \text{ erg.} \quad (1)$$

The burst spectrum can be fitted with a blackbody plus power-law model (Li et al. 2020).

2.2. FRB 200428

On 2020 April 28, The CHIME/FRB Collaboration et al. (2020) detected a luminous millisecond radio burst at 400–800 MHz, which was considered to be spatially and temporally coincident with the hard XRB from SGR 1935+2154 (The CHIME/FRB Collaboration et al. 2020). Meanwhile, the Survey for Transient Astronomical Radio Emission 2 (STARE2) radio array also observed this millisecond-duration radio burst (Bochenek et al. 2020). The radio burst detected by the Canadian Hydrogen Intensity Mapping Experiment (CHIME) radio telescope at 400–800 MHz consists of two subbursts with best-fit temporal widths of 0.585 ± 0.014 ms and 0.335 ± 0.007 ms separated by 28.91 ± 0.02 ms (The CHIME/FRB Collaboration et al. 2020). According to The CHIME/FRB Collaboration et al. (2020), the average fluence of 480 kJy ms for the first component and 220 kJy ms for the second were reported. The band-average peak flux density was 110 kJy for the first component and 150 kJy for the second, respectively. The value of the DM along the direction of FRB 200428 is 332.7206 ± 0.0009 pc cm $^{-3}$.

Another observation of FRB 200428 comes from the STARE2 radio array in the 1281–1468 MHz band (Bochenek et al. 2020). The burst was detected with an intrinsic width of 0.61 ms. The band-averaged fluence is 1.5×10^6 Jy ms. The isotropic energy of FRB 200428 observed by STARE2 is

$$E_{\text{FRB}} = 4\pi F_\nu d^2 \nu_c = 2 \times 10^{35} \text{ erg,} \quad (2)$$

where F_ν is the fluence of FRB 200428 and the center frequency of STARE2 $\nu_c = 1.4$ GHz (Bochenek et al. 2020). The isotropic-equivalent energies of two subbursts detected by CHIME are 2.6×10^{34} erg and 1.2×10^{34} erg, respectively.

Here we assume the center frequency of CHIME is 600 MHz. The brightness temperature 10^{32} K is similar to that of cosmological FRBs (Bochenek et al. 2020). It has been confirmed that FRB 200428 is temporally and spatially consistent with the XRB and they both have substructure (Li et al. 2020; Ridnaia et al. 2020). The energy ratio between FRB 200428 and the XRB from SGR 1935+2154 is

$$\eta \equiv \frac{E_{\text{FRB}}}{E_X} \sim 10^{-5}. \quad (3)$$

3. Constraints on Model Parameters

For the synchrotron maser shock model, the radiation can be powered by a relativistic shock propagating into a moderately magnetized ($\sigma > 10^{-3}$) upstream medium (Lyubarsky 2014; Beloborodov 2017; Metzger et al. 2019). Nevertheless, the properties of shocks and the composition of the upstream medium are widely discussed. So far, three cases have been proposed, including that the upstream is a rotationally powered pulsar wind (Beloborodov 2017), a magnetar wind nebula (Lyubarsky 2014), or a baryonic shell (Metzger et al. 2019). In the model of Metzger et al. (2019), during a magnetar XRB, the ejecta with two components will be launched. The initial ultrarelativistic (Γ_{ej}) one with high magnetization may be driven by the engine that triggers the XRB to power the FRB. This ultrarelativistic component may consist of electron–positron pairs, as suggested by Yu et al. (2020). The other is a more prolonged phase of ion-loaded mass loss with a subrelativistic velocity $\beta_w = v_w/c < 1$, which provides the upstream medium to generate the FRB.

We use the observations of FRB 200428 and the associated XRB to constrain the parameters of this model. From the observations, the XRB associated with FRB 200428 is similar to other XRBs of SGR 1935+2154 (Lin et al. 2020b). Therefore, we assume that it occurs in the magnetosphere to trigger the mass ejection. Unlike Margalit et al. (2020a), they assumed that the XRB is mainly produced by the relativistic hot electrons, similar to gamma-ray burst afterglows. The radiation efficiency ζ for converting the kinetic energy of the ejecta into coherent radio radiation in the baryonic shell can be simulated as (Metzger et al. 2019)

$$\begin{aligned} \zeta \approx & 4.8 \times 10^{-4} \left(\frac{E_X}{9.4 \times 10^{39} \text{ erg}} \right)^{-4/5} \\ & \times \left(\frac{E_{\text{FRB}}}{2 \times 10^{35} \text{ erg}} \right)^{4/5} \left(\frac{m_*}{m_e} \right)^{1/2} \left(\frac{f_e}{0.5} \right)^{-1/4} \\ & \times \left(\frac{\nu_{\text{FRB}}}{1.4 \text{ GHz}} \right)^{1/4} \left(\frac{t_{\text{FRB}}}{0.61 \text{ ms}} \right)^{1/4}, \end{aligned} \quad (4)$$

where E_X and E_{FRB} are the energy releases of the XRB and FRB 200428 detected by STARE2, respectively. In the following, the observation of STARE2 is used. We assumed that the energy of XRB approximately equals the energy carried by the ultrarelativistic ejecta. m_* is the effective mass, and f_e is defined as the ratio of electron density to external particle density, i.e., $f_e \equiv n_e/n_{\text{ext}}$. For the upstream medium of electron–ion composition, we suppose $f_e \simeq 0.5$. The predicted radiation efficiency ζ can explain the observed one (Equation (3)).

We assume the intrinsic synchrotron maser efficiency $f_\xi = 10^{-3}$ (Metzger et al. 2019). Using the observed frequency ν_{FRB} , fluence F_ν , and duration t_{FRB} , we can solve the Lorentz factor Γ of the shocked gas, the radius of shock r_{sh} , and the external density of the medium at r_{sh} as follows:

$$\begin{aligned} \Gamma &\approx 53.4 \left(\frac{m_*}{m_e} \right)^{1/30} \left(\frac{f_e}{0.5} \right)^{1/15} \\ &\times \left(\frac{f_\xi}{10^{-3}} \right)^{-1/15} \left(\frac{\nu_{\text{FRB}}}{1.4 \text{ GHz}} \right)^{-7/30} \\ &\times \left(\frac{t_{\text{FRB}}}{0.61 \text{ ms}} \right)^{-2/5} \left(\frac{E_{\text{FRB}}}{2 \times 10^{35} \text{ erg}} \right)^{1/6}, \end{aligned} \quad (5)$$

$$\begin{aligned} r_{\text{sh}} &\approx 2\Gamma^2 ct \approx 9.9 \times 10^{10} \text{ cm} \left(\frac{m_*}{m_e} \right)^{1/15} \\ &\times \left(\frac{f_e}{0.5} \right)^{2/15} \left(\frac{f_\xi}{10^{-3}} \right)^{-2/15} \\ &\times \left(\frac{\nu_{\text{FRB}}}{1.4 \text{ GHz}} \right)^{-7/15} \left(\frac{t_{\text{FRB}}}{0.61 \text{ ms}} \right)^{1/5} \left(\frac{E_{\text{FRB}}}{2 \times 10^{35} \text{ erg}} \right)^{1/3}, \end{aligned} \quad (6)$$

$$\begin{aligned} n_{\text{ext}}(r_{\text{sh}}) &\approx 1.8 \times 10^4 \text{ cm}^{-3} \left(\frac{m_*}{m_e} \right)^{2/15} \\ &\times \left(\frac{f_e}{0.5} \right)^{-11/15} \left(\frac{f_\xi}{10^{-3}} \right)^{-4/15} \\ &\times \left(\frac{\nu_{\text{FRB}}}{1.4 \text{ GHz}} \right)^{31/30} \left(\frac{t_{\text{FRB}}}{0.61 \text{ ms}} \right)^{2/5} \left(\frac{E_{\text{FRB}}}{2 \times 10^{35} \text{ erg}} \right)^{-1/3}. \end{aligned} \quad (7)$$

The induced Compton scattering (ICS) will suppress the short radio bursts. Only the optical depth of the induced Compton scattering τ_{ICS} is smaller than 3; radio radiation can escape from the baryonic shell (Metzger et al. 2019). When the optical depth equals 3, the corresponding frequency is defined as the peak frequency of the observed spectrum, i.e., $\nu_{\text{max}} \equiv \nu(\tau_{\text{ICS}} = 3)$. Thus, ν_{max} can be expressed as

$$\begin{aligned} \nu_{\text{max}} &= 0.97 \text{ GHz} \left(\frac{f_\xi}{10^{-3}} \right)^{1/4} \left(\frac{E_{\text{FRB}}}{2 \times 10^{35} \text{ erg}} \right)^{5/32} \\ &\times \dot{M}_{21}^{15/32} \left(\frac{\beta_w}{0.3} \right)^{-45/32} \\ &\times \Delta T_4^{-30/32} \left(\frac{t_{\text{FRB}}}{0.61 \text{ ms}} \right)^{-7/32} \left(\frac{f_e}{0.5} \right)^{5/8}, \end{aligned} \quad (8)$$

where $\Delta T = 10^4 \text{ s}$ is the time interval between the successive XRBs and $\beta_w = 0.3$ is assumed. And $\dot{M} = 10^{21} \text{ g s}^{-1}$ is the electron-ion injection rate.

From observations, the separation time of the two narrow X-ray peaks is consistent with that of the two peaks in FRB 200428 (Li et al. 2020). After correcting the dispersion time delay by 333 pc cm^{-3} , the two X-ray peaks each occur within about $t_\delta \sim 1 \text{ ms}$ of the corresponding CHIME burst peaks (Li et al. 2020; The CHIME/FRB Collaboration et al. 2020). Therefore, the Lorentz factor Γ_{ej} of the ultrarelativistic

component is required to satisfy

$$\begin{aligned} \Gamma_{\text{ej}} &\geq (r_{\text{sh}}/2ct_\delta)^{1/2} \\ &\approx 40.7 \left(\frac{r_{\text{sh}}}{9.9 \times 10^{10} \text{ cm}} \right)^{1/2} \left(\frac{t_\delta}{1 \text{ ms}} \right)^{1/2}. \end{aligned} \quad (9)$$

Incoherent synchrotron afterglow is also produced by the relativistic hot electrons, which is similar to the gamma-ray burst afterglow (Lyubarsky 2014; Metzger et al. 2019). The peak frequency of the synchrotron afterglow is given by (Metzger et al. 2019)

$$\begin{aligned} h\nu_{\text{syn}} &\approx 552.6 \text{ keV} \left(\frac{E_X}{9.4 \times 10^{39} \text{ erg}} \right)^{1/2} \\ &\times \left(\frac{t}{1 \text{ ms}} \right)^{-3/2} \left(\frac{\sigma}{10^{-2}} \right)^{1/2}, \end{aligned} \quad (10)$$

where $\sigma = 10^{-2}$ and t is the time since the XRB peak. It is obvious that this peak frequency is similar to that of the XRB occurring in the magnetar's magnetosphere. Therefore, this emission may overlap the original XRB in the magnetosphere. Margalit et al. (2020a) assumed the XRB is mainly from the synchrotron afterglow. The observational properties of FRB 200428 can be well explained in these two physical scenarios. The radio burst properties are similar in the magnetosphere-powered situation and the shock-powered situation. The predicted shock-powered X-ray fluence is close to the observed one (Margalit et al. 2020a), which indicates that part of the XRB may come from shock emission. Thus, the magnetospheric XRBs and the shock-powered XRBs may coexist in this model.

The relative time delay t_δ between the XRB and the radio burst is about $r_{\text{sh}}/\Gamma_{\text{ej}}^2 c \sim \text{ms}$, which is comparable to the radio burst duration. From observations, CHIME (The CHIME/FRB Collaboration et al. 2020) and Insight-HXMT (Li et al. 2020) found that the two X-ray peaks each occurred within 1 ms of the arrival times of the radio peaks detected by CHIME, which is consistent with our estimation.

4. Energy Frequency Distributions

In the synchrotron maser model proposed by Metzger et al. (2019), the energy of FRBs is proportional to the kinetic energy carried by ultrarelativistic ejecta, if the upstream magnetization is similar. The kinetic energy of ultrarelativistic ejecta has the same order of that of the corresponding XRB (Yu et al. 2020). For a magnetar, the magnetization of the upstream medium may not change significantly. Therefore, it is expected that the occurrence of frequency distributions of energy for XRBs and the associated FRBs are similar. Only a portion of XRBs is associated with FRBs. For example, no bursts are found from SGR 1935+2154 by eight-hour observation of the Five-hundred-meter Aperture Spherical Telescope (FAST; Lin et al. 2020b). However, there are 29 XRBs of SGR 1935+2154 in the same period (Lin et al. 2020b). The possible reason is the beaming emission of FRBs.

The cumulative energy distribution of FRB 121102 was considered to have a power-law form. Law et al. (2017) found that the slope of differential distribution of energy is ~ 1.7 using multi-telescope detection. Gourdji et al. (2019) found the cumulative distribution of burst energies with a slope of 1.8 ± 0.3 . Furthermore, Wadiasingh & Timokhin (2019)

obtained a differential energy distribution with a power-law index of 2.3 ± 0.2 using 72 bursts.

We compare the energy occurrence distribution between FRBs and XRBs of SGRs. The data of FRB 121102 (Zhang et al. 2018) and magnetar SGR 1935+2154 (Lin et al. 2020a) are used. We use a power-law distribution with a high-energy cutoff to fit the cumulative distribution, which reads

$$N(>E) = A(E^{1-\alpha_E} - E_{\max}^{1-\alpha_E}), \quad (11)$$

where α_E is the power-law index and E_{\max} is the maximum energy of the FRB. Using Equation (11), Cheng et al. (2020) found that the power-law index of the energy frequency distribution of 93 bursts of FRB 121102 is $\alpha_E = 1.63 \pm 0.06$. For SGR 1935+2154, the 112 bursts observed by Fermi/GBM from 2014 to 2016 are used. The power-law index of energy distribution for SGR 1935+2154 is $\alpha_E = 1.71 \pm 0.03$. The two distributions are consistent with each other at the 1σ confidence level, which supports the association between XRBs and FRBs.

5. Rotation Measure and Persistent Radio Source

The intermittent injection of ejecta from a magnetar will generate an expanding magnetized electron-ion nebula. Observations show that a luminous ($\nu L_\nu = 10^{39} \text{ erg s}^{-1}$) persistent radio source coincident to within $\leq 40 \text{ pc}$ of the FRB 121102 location (Marcote et al. 2017). Meanwhile, the high rotation measure (RM) of the bursts, $\text{RM} \sim 10^5 \text{ rad m}^{-2}$, is found (Michilli et al. 2018). The persistent radio emission and high RM may originate from the same medium, showing that the FRB source is embedded in a dense magnetized plasma (Michilli et al. 2018). The persistent radio source is thought to be synchrotron radiation of the magnetar wind nebula (Dai et al. 2017; Kashiyama & Murase 2017; Metzger et al. 2017). For the Galactic magnetar SGR 1935+2154, the extended X-ray emission was found by Israel et al. (2016) and can be interpreted as a pulsar wind nebula. But Younes et al. (2017) found that there was no extended emission around SGR 1935+2154 using Chandra data. For the XMM-Newton data, they found similar results as Israel et al. (2016). So there is marginal evidence of the existence of a magnetar wind nebula around SGR 1935+2154. Below, we assume the magnetar wind nebula is around the source. Kothes et al. (2018) discovered a bright radio shell consists of two narrow arc-like features and a radial magnetic field around SGR 1935+2154, which could be explained by a pulsar wind nebula (Kothes et al. 2018). On the other hand, it could also be explained as interaction of the SNR with the ambient medium. Here, we only consider the former case. The spectrum of the radio emission is $S_\nu \propto \nu^{-0.55 \pm 0.02}$ (Kothes et al. 2018), which is similar to that of the persistent radio source of FRB 121102 ($\nu^{-0.27 \pm 0.24}$; Marcote et al. 2017). The luminosity of the radio shell associated with SGR 1935+2154 is $5 \times 10^{33} \text{ erg s}^{-1}$ (Kothes et al. 2018). The RM toward the direction of SGR 1935+2154 is about $116 \pm 2 \pm 5 \text{ rad m}^{-2}$ (The CHIME/FRB Collaboration et al. 2020; Zhang et al. 2020).

It has been shown that the persistent radio source associated with FRB 121102 can be explained by a single expanding magnetized electron-ion wind nebula created by magnetar flares (Margalit & Metzger 2018). Assuming that the radio shell emission around SGR 1935+2154 is also powered by a pulsar wind nebula, we explain the observations (radio

luminosity and RM) using the model proposed by Margalit & Metzger (2018). Considering the magnetar releases its free magnetic energy into the nebula in a power-law form (Margalit & Metzger 2018)

$$\dot{E} \propto t^{-\alpha}, \quad (12)$$

the time evolution of RM is

$$\text{RM} \propto t^{-(6+\alpha)/2}, \quad (13)$$

and the decay of radio source luminosity is

$$\nu L_\nu \propto t^{-(\alpha^2+7\alpha-2)/4}. \quad (14)$$

The age of the magnetar powering FRB 121102 is found to be very young, i.e., a few decades to 100 yr (Cao et al. 2017; Kashiyama & Murase 2017; Metzger et al. 2017). We take 100 yr as a fiducial value. So the luminosity of the magnetar wind nebula is $10^{39} \text{ erg s}^{-1}$ at $t = 100 \text{ yr}$. The age of SGR 1935+2154 is about 16,000 yr from nondetection of thermal X-ray emission from the supernova remnant and the relatively dense environment (Zhou et al. 2020). In order to explain the observations of RM and radio source luminosity for FRB 121102, $\alpha = 1.3 - 1.8$ is adopted (Margalit & Metzger 2018). For $\alpha = 1.37$, the persistent radio source luminosity is about $\nu L_\nu = 6.1 \times 10^{33} \text{ erg s}^{-1}$ at $t = 16,000 \text{ yr}$, which is extremely consistent with the observed one of SGR 1935+2154. For RM, the value is $8 \times 10^{-4} \text{ rad m}^{-2}$ at $t = 16,000 \text{ yr}$. It is also consistent with the FAST observation. From a highly polarized radio burst from SGR 1935+2154, it is found that the RM contribution from the local magnetoionic environment is very low (Zhang et al. 2020). In Figure 1, we show the time evolution of the persistent radio source luminosity and RM for FRB 121102 and FRB 200428.

Figure 1 also show the observations of FRB 180916 as blue pentagons, which was located in a nearby massive spiral galaxy (Marcote et al. 2020). From the VLA data, the persistent radio source luminosity of FRB 180916.J0158+65 was constrained to $\nu L_\nu < 7.6 \times 10^{35} \text{ erg s}^{-1}$. Based on the time evolution of the persistent radio source, we find that the lower limit of age for the central magnetar is about 2079 yr. Using this age, the RM is about 1.4 rad m^{-2} , which is also consistent with observations of CHIME/FRB Collaboration et al. (2019). CHIME/FRB Collaboration et al. (2019) measured the RM of FRB 180916 as $-114.6 \pm 0.6 \text{ rad m}^{-2}$. The observed RM_{tot} consists of the contribution of the Milky Way, the host galaxy, and the source. In the direction of the FRB 180916, the contribution of the RM from the Milky Way is $-115 \pm 12 \text{ rad m}^{-2}$ (Ordog et al. 2019). Therefore, the major contribution to the RM value of FRB 180916 comes from the Milky Way, while the contribution of the FRB source and the host galaxy can be as small as a few rad m^{-2} .

Therefore, the RM and radio source luminosity of FRB 121102, FRB 200428, and FRB 180916 can be well understood in a single expanding magnetized electron-ion wind nebula embedded within a supernova remnant.

6. Baryon Mass Budget

In the model proposed by Metzger et al. (2019), the FRBs are produced in the collision between the ultrarelativistic ejecta and the external baryonic shell ejected by the previous flare. The baryonic mass required for producing one cosmological

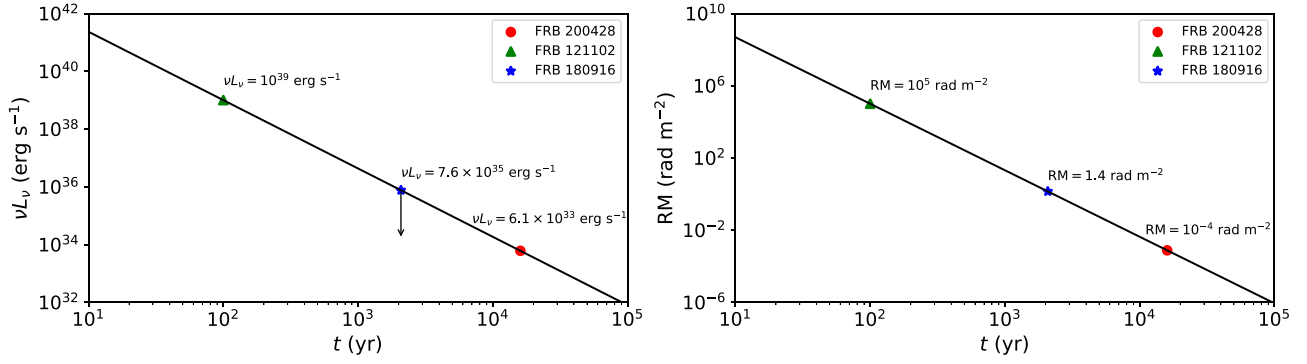


Figure 1. Time evolution of persistent radio source luminosity (νL_ν ; left panel) and RM value (right panel). Red dot is for FRB 200428, green triangle is for FRB 121102, and blue pentagon is for FRB 180916. In the left panel, the blue pentagon represents the upper limit of the persistent radio source luminosity of FRB 180916 from Equation (14). In order to explain the upper limit of the persistent radio source luminosity of FRB 180916, the central magnetar age must be larger than about 2000 yr. Using this lower limit of central magnetar age for FRB 180916, the model-predicted RM (Equation (13)) is about 1.4 rad m^{-2} , which is consistent with the observation.

FRB is about $\Delta M = \dot{M} \Delta T$, where $\dot{M} \sim 10^{19} - 10^{21} \text{ g s}^{-1}$ and $\Delta T \sim 10^4 \text{ s}$ is the time interval between the successive XRBs (Metzger et al. 2019). For Galactic FRB 200428, a low value $\Delta M \sim 10^{20} \text{ g}$ is required (Yu et al. 2020). An important question is whether the magnetar can supply so much baryonic material. Using the observation of FRB 121102, we give an estimation of the baryonic mass required by this model.

We use the data of FRB 121102 observed by the Green Bank Telescope (GBT; Zhang et al. 2018), which is the largest sample in a single observation. There are 93 bursts in 5 hr observation. The energy of each burst can be derived from

$$E = 4\pi d_l^2 F \nu_c, \quad (15)$$

where d_l is the luminosity distance at $z = 0.19$, F is the fluence, and ν_c is the center frequency of GBT (Zhang et al. 2018). The Λ CDM model with $H_0 = 67.74 \text{ km s}^{-1} \text{ Mpc}^{-1}$, $\Omega_M = 0.31$, and $\Omega_\Lambda = 0.69$ is used. The total energy release in these five hours is $E_t = \sum_i E_i$, where E_i the energy of i th burst. Rajwade et al. (2020) found a possible period of 157 days with a duty cycle of 56%. If this observation is in the active phase of FRB 121102, the energy release in a period can be derived as

$$E_{\text{radio}} = \frac{E_t}{T_{\text{obs}}} T_{\text{period}} \xi \simeq 1.8 \times 10^{43} \text{ erg}, \quad (16)$$

where $T_{\text{obs}} = 5 \text{ hr}$ is the observation time, $T_{\text{period}} = 157 \text{ days}$ is the period, and $\xi = 0.56$ is the duty cycle.

The observation of FRB 200428 suggests the FRBs are accompanied by XRBs. The energy ratio between radio burst and XRB is about $\eta \sim 10^{-5}$. If this value is valid for FRB 121102, the X-ray energy release in one period for FRB 121102 is about

$$E_X = \frac{E_{\text{radio}}}{\eta} \simeq 1.8 \times 10^{48} \text{ erg} \left(\frac{\eta}{10^{-5}} \right)^{-1}. \quad (17)$$

The typical active timescale of magnetars is about 100 yr (Beloborodov & Li 2016). The total energy release of XRBs in the active phase is

$$E_{\text{total}} = \frac{\tau}{T_{\text{period}}} E_X \simeq 4.2 \times 10^{50} \times \text{erg} \left(\frac{\eta}{10^{-5}} \right)^{-1} \left(\frac{\tau}{100 \text{ yr}} \right), \quad (18)$$

where τ is the active timescale of the magnetar. For FRB 121102, $\tau \sim 100 \text{ yr}$ is assumed. Compared to the rotational energy, the magnetic energy is the main reservoir responsible for powering FRBs. The magnetic energy of magnetar is

$$E_B \simeq B^2 R^3 / 6 \approx 3 \times 10^{49} \text{ erg } B_{16}^2, \quad (19)$$

where $B = 10^{16} \text{ G}$ is the interior magnetic field strength, and $R = 12 \text{ km}$ is the magnetar radius. This value is smaller than the required XRB energy. The XRB energy is shared by the ultrarelativistic ejecta and the baryon shell with a subrelativistic velocity v_w . It has been found that the kinetic energy of the baryon shell is comparable to the flare energy (Metzger et al. 2019; Margalit et al. 2020b). We assume that the baryon shell is subrelativistic with a typical velocity $v_w = 0.3c$. Based on the above assumptions, the baryonic mass ejected by magnetar in the active time can be derived as

$$M_B \simeq 2 \frac{E_{\text{total}}}{v_w^2} \simeq 5.2 \times 10^{-3} M_\odot \times \left(\frac{\eta}{10^{-5}} \right)^{-1} \left(\frac{\tau}{100 \text{ yr}} \right) \left(\frac{v_w}{0.3c} \right)^{-2}. \quad (20)$$

This value is much larger than the typical mass ($10^{-5} M_\odot$) of a magnetar outer crust (Gudmundsson et al. 1983; Glendenning & Weber 1992). According to the structure of magnetars, the core is mainly composed of superfluid. The ejected baryon matter of the magnetar is mainly provided by crust. The baryonic mass estimated in this model is larger than the typical mass of a magnetar outer crust, indicating that the outer crust of the magnetar cannot eject enough baryonic matter required by the model. In Figure 2, we show the constraints on M_B using Equation (20). If the radiation efficiency $\eta = 10^{-5}$ from FRB 200428 is used, the required baryonic mass M_B is always larger than $10^{-5} M_\odot$ for the whole parameter ranges as shown in the left panel of Figure 2. If $\tau = 100 \text{ yr}$ is fixed, the same result is shown in the right panel of Figure 2. The outer crust of magnetars is not sufficient to provide such a large baryonic mass, which challenges the synchrotron maser shock model. Interestingly, if the inner crust is included, the total mass of crust is about $0.01 M_\odot$ (Chamel & Haensel 2008), which is larger than the required baryonic mass. Theoretically, the

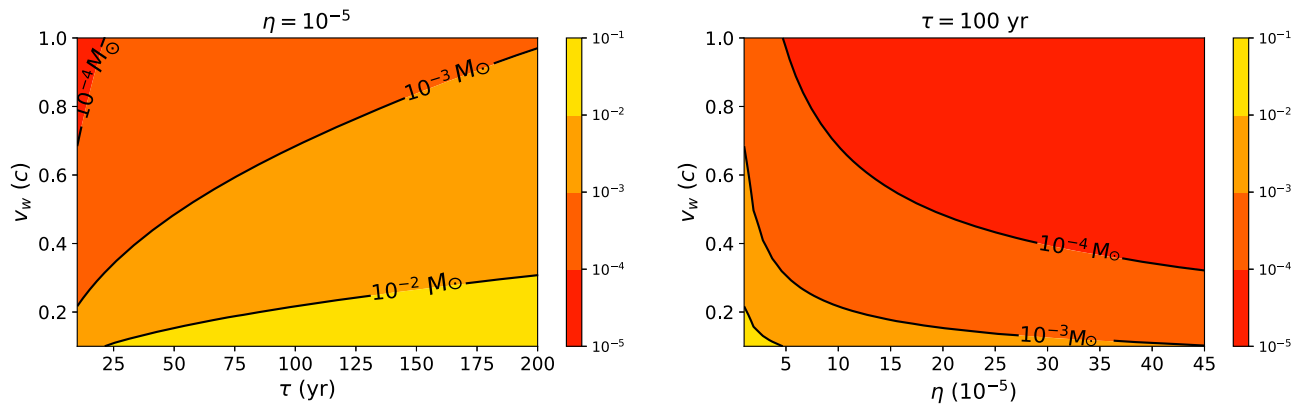


Figure 2. Constraints on the required baryonic mass M_B in the $\tau - v_w$ plane (left panel) and $\eta - v_w$ plane (right panel). In the left panel, $\eta = 10^{-5}$ is fixed. The value of M_B is larger than $10^{-3}M_\odot$ for the whole range of parameters. In the right panel, $\tau = 100$ yr is fixed. The value of M_B is larger than $10^{-5}M_\odot$ for the whole range of parameters.

physical mechanism and the rate of the baryonic mass ejection are both uncertain. More investigations are required. We also use the bursts of FRB 121102 observed by FAST to estimate the required baryonic mass (Li et al. 2019). The observation of FAST provides the information on the lowest-energy bursts of FRB 121102 so far. In a 56.5 hr observation, 1121 bursts were observed. The total energy of these bursts is 3.14×10^{41} erg.³ Therefore, the average energy release in one period is about 1.18×10^{43} erg. Using the same formulae as above, the baryon mass can be approximated as

$$M_B \sim 3.5 \times 10^{-3} M_\odot \left(\frac{\eta}{10^{-5}} \right)^{-1} \left(\frac{\tau}{100\text{yr}} \right) \left(\frac{v_w}{0.3c} \right)^{-2}, \quad (21)$$

which is similar to that derived from GBT observation.

The required baryonic mass can also be roughly derived by $\dot{M} \times \tau$. For $\dot{M} \sim 10^{19} - 10^{21}$ g s⁻¹ and $\tau = 100$ yr, the mass is between 1.5×10^{-5} to $1.5 \times 10^{-3} M_\odot$, which covers two orders of magnitude. The largest value is comparable to our result, i.e., Equation (20). The smallest value is similar to the mass of magnetar outer crust. However, the bursts of FRB 121102 occur in an irregular fashion, and appear to be clustered (Wang & Yu 2017; Oppermann et al. 2018). So this calculation is an approximation. In order to obtain a precise value, the period and duty cycle of bursts must be considered.

7. Summary

Motivated by the fact that FRB 200428 is spatially and temporally coincident with a hard XRB from SGR 1935+2154, we test the synchrotron maser shock model in this Letter. Our conclusions can be summarized as follows.

(1) Here we consider the case that the upstream medium is electron-ion material. We find that the radiation efficiency, Lorentz factor of shocked gas, the radius of shock, and the density of the external medium are consistent with the upstream medium, which is an ion-loaded shell released by a recent burst.

(2) Similar energy occurrence frequency distributions between bursts of FRB 121102 and XRBs of SGR 1935+2154 are found, which supports the association of FRBs and XRBs from magnetars.

(3) In this model, the energy injection by intermittent ejecta from the magnetar will generate an expanding magnetized electron-ion nebula. We show that the radio continuum emission around SGR 1935+2154 can be well understood in the magnetar nebula model, by assuming the same energy injection rate $\dot{E} \propto t^{-1.37}$ as FRB 121102.

(4) The RM value contributed by the nebula is 8×10^{-4} rad m⁻². This small value is consistent with the observation that the main contribution of RM is the interstellar medium between SGR 1935+2154 and us. Therefore, all of the observational properties of FRB 200428 can be well understood in the synchrotron maser shock model.

(5) However, in order to explain the observations, the upstream medium must be an ion-loaded shell. To study whether the magnetar can provide enough baryonic matter, we use the observation of FRB 121102 from GBT and FAST to estimate the required baryonic mass. The baryon mass ejected by the central magnetar in an active lifetime is about $5.2 \times 10^{-3} M_\odot$ using the GBT observation, which is much larger than the typical mass of a magnetar outer crust. FAST observation gives a similar result. So the large baryonic mass challenges this model. If both the outer and inner crusts are considered, the mass of crust is about $0.01 M_\odot$, which is enough for the required baryonic mass.

We thank Y. W. Yu, S. L. Xiong, P. Wang, P. Zhou, D. Li., and X. Y. Li for helpful discussions. We thank the anonymous referee for valuable comments. This work is supported by the National Natural Science Foundation of China (grants U1831207 and 11833003), and the National Key Research and Development Program of China (grant 2017YFA0402600).

ORCID iDs

Q. Wu <https://orcid.org/0000-0001-6021-5933>
 G. Q. Zhang <https://orcid.org/0000-0001-6545-4802>
 F. Y. Wang <https://orcid.org/0000-0003-4157-7714>
 Z. G. Dai <https://orcid.org/0000-0002-7835-8585>

References

- Bastian, T. S., Benz, A. O., & Gary, D. E. 1998, *ARA&A*, **36**, 131
 Beloborodov, A. M. 2017, *ApJL*, **843**, L26
 Beloborodov, A. M., & Li, X. 2016, *ApJ*, **833**, 261
 Bochenek, C. D., Ravi, V., Belov, K. V., et al. 2020, arXiv:2005.10828

³ D. Li & P. Wang 2020, private communications.

- Cao, X.-F., Yu, Y.-W., & Dai, Z.-G. 2017, *ApJL*, 839, L20
- Chamel, N., & Haensel, P. 2008, *LRR*, 11, 10
- Cheng, Y., Zhang, G. Q., & Wang, F. Y. 2020, *MNRAS*, 491, 1498
- CHIME/FRB Collaboration, Andersen, B. C., Bandura, K., et al. 2019, *ApJL*, 885, L24
- Cordes, J. M., & Chatterjee, S. 2019, *ARA&A*, 57, 417
- Dai, Z. G. 2020, *ApJL*, 897, L40
- Dai, Z. G., Wang, J. S., & Yu, Y. W. 2017, *ApJL*, 838, L7
- Hurley, J.-J., Li, B., Li, L.-B., et al. 2020, *ApJL*, 898, L55
- Glendenning, N. K., & Weber, F. 1992, *ApJ*, 400, 647
- Gourdji, K., Michilli, D., Spitler, L. G., et al. 2019, *ApJL*, 877, L19
- Gudmundsson, E. H., Pethick, C. J., & Epstein, R. I. 1983, *ApJ*, 272, 286
- Hurley, K., Mitrofanov, I. G., Golovin, D., et al. 2020, *GCN*, 27625, 1
- Israel, G. L., Esposito, P., Rea, N., et al. 2016, *MNRAS*, 457, 3448
- Kashiyama, K., & Murase, K. 2017, *ApJL*, 839, L3
- Katz, J. I. 2016, *ApJ*, 826, 226
- Katz, J. I. 2020, arXiv:2006.03468
- Kothes, R., Sun, X., Gaensler, B., & Reich, W. 2018, *ApJ*, 852, 54
- Kulkarni, S. R., Ofek, E. O., Neill, J. D., Zheng, Z., & Juric, M. 2014, *ApJ*, 797, 70
- Law, C. J., AbruZZo, M. W., Bassa, C. G., et al. 2017, *ApJ*, 850, 76
- Li, C. K., Lin, L., Xiong, S. L., et al. 2020, arXiv:2005.11071
- Li, Y., Zhang, B., Nagamine, K., & Shi, J. 2019, *ApJL*, 884, L26
- Lien, A. Y., Barthelmy, S. D., Baumgartner, W. H., et al. 2014, *GCN*, 16522, 1
- Lin, L., Göğüş, E., Roberts, O. J., et al. 2020a, *ApJ*, 893, 156
- Lin, L., Zhang, C. F., Wang, P., et al. 2020b, arXiv:2005.11479
- Lorimer, D. R., Bailes, M., McLaughlin, M. A., Narkevic, D. J., & Crawford, F. 2007, *Sci*, 318, 777
- Lu, W., & Kumar, P. 2018, *MNRAS*, 477, 2470
- Lu, W., Kumar, P., & Zhang, B. 2020, arXiv:2005.06736
- Lyubarsky, Y. 2014, *MNRAS*, 442, L9
- Lyutikov, M., & Popov, S. 2020, arXiv:2005.05093
- Marcote, B., Nimmo, K., Hessels, J. W. T., et al. 2020, *Natur*, 577, 190
- Marcote, B., Paragi, Z., Hessels, J. W. T., et al. 2017, *ApJL*, 834, L8
- Margalit, B., Beniamini, P., Sridhar, N., & Metzger, B. D. 2020a, *ApJL*, 899, L27
- Margalit, B., & Metzger, B. D. 2018, *ApJL*, 868, L4
- Margalit, B., Metzger, B. D., & Sironi, L. 2020b, *MNRAS*, 494, 4627
- Mereghetti, S., Savchenko, V., Ferrigno, C., et al. 2020, *ApJL*, 898, L29
- Metzger, B. D., Berger, E., & Margalit, B. 2017, *ApJ*, 841, 14
- Metzger, B. D., Margalit, B., & Sironi, L. 2019, *MNRAS*, 485, 4091
- Michilli, D., Seymour, A., Hessels, J. W. T., et al. 2018, *Natur*, 553, 182
- Murase, K., Kashiyama, K., & Mészáros, P. 2016, *MNRAS*, 461, 1498
- Oppermann, N., Yu, H.-R., & Pen, U.-L. 2018, *MNRAS*, 475, 5109
- Ordog, A., Booth, R., van Eck, C., Brown, J.-A., & Landecker, T. 2019, *Galax*, 7, 43
- Petroff, E., Hessels, J. W. T., & Lorimer, D. R. 2019, *A&ARv*, 27, 4
- Platts, E., Weltman, A., Walters, A., et al. 2019, *PhR*, 821, 1
- Popov, S. B., & Postnov, K. A. 2013, arXiv:1307.4924
- Rajwade, K. M., Mickaliger, M. B., Stappers, B. W., et al. 2020, *MNRAS*, 494, 3551
- Reid, H. A. S., & Ratcliffe, H. 2014, *RAA*, 14, 773
- Ridnaia, A., Svinkin, D., Frederiks, D., et al. 2020, arXiv:2005.11178
- Stamatikos, M., Malesani, D., Page, K. L., & Sakamoto, T. 2014, *GCN*, 16520, 1
- Tavani, M., Casentini, C., Ursi, A., et al. 2020, arXiv:2005.12164
- The CHIME/FRB Collaboration, Andersen, B. C., Bandura, K. M., et al. 2020, arXiv:2005.10324
- Thornton, D., Stappers, B., Bailes, M., et al. 2013, *Sci*, 341, 53
- Veres, P., Bissaldi, E., Briggs, M. S. & Fermi GBM Team 2020, *GCN*, 27531, 1
- Wadiasingh, Z., & Timokhin, A. 2019, *ApJ*, 879, 4
- Wang, F. Y., Wang, Y. Y., Yang, Y.-P., et al. 2020, *ApJ*, 891, 72
- Wang, F. Y., & Yu, H. 2017, *JCAP*, 03, 023
- Wang, J.-S. 2020, arXiv:2006.14503
- Yang, Y.-P., & Zhang, B. 2018, *ApJ*, 868, 31
- Yang, Y.-P., Zhu, J.-P., Zhang, B., & Wu, X.-F. 2020, arXiv:2006.03270
- Younes, G., Kouveliotou, C., Jaodand, A., et al. 2017, *ApJ*, 847, 85
- Yu, Y.-W., Zou, Y.-C., Dai, Z.-G., & Yu, W.-F. 2020, arXiv:2006.00484
- Zhang, C. F., Jiang, J. C., Men, Y. P., et al. 2020, *ATel*, 13699, 1
- Zhang, G. Q., Wang, F. Y., & Dai, Z. G. 2019, arXiv:1903.11895
- Zhang, Y. G., Gajjar, V., Foster, G., et al. 2018, *ApJ*, 866, 149
- Zhong, S.-Q., Dai, Z.-G., Zhang, H.-M., & Deng, C.-M. 2020, *ApJL*, 898, L5
- Zhou, P., Zhou, X., Chen, Y., et al. 2020, arXiv:2005.03517